Self-Assembled Chromogen-loaded Polymeric Cocoon for Respiratory Virus Detection

ARTICLE

Self-Assembled Chromogen-loaded Polymeric Cocoon for Respiratory Virus Detection

Received 00th January 20xx,
Accepted 00th January 20xx

DOI: 10.1039/x0xx00000x

www.rsc.org/

Indra Memdi Khoris[1,†], Akhilesh Babu Ganganboina[2,†], Tetsuro Suzuki[3], Enoch Y. Park[1,2*]

Inspired by the self-assembly approach, in this work, the chromogen, 3,3',5,5'-tetramethylbenzidine (TMB), is successfully co-precipitated in the aqueous solution to form collective nanoparticles (NPs) of signal molecules (TMB-NPs). Utilizing the poly(lactide-co-glycolide) (PLGA) in the molecular delivery approach, the formed emulsion nanovesicle (TMB-NPs@PLGA) has an enrichment of the collective signal molecules in a single antibody-antigen conjugation. A specific antibody-conjugated TMB-NPs@PLGA forms an immunocomplex sandwich structure upon the addition of the influenza virus (IV)/A. The addition of dimethyl sulfoxide (DMSO) dissolves the PLGA nanovesicles, releasing the encapsulated TMB-NPs. Sequentially, the TMB-NPs release TMB molecules by the DMSO. The released TMB is catalytically oxidized by H_2O_2 with self-assembled protein-inorganic nanoflower, copper nanoflowers (CuNFs) as the nanozyme. The developed immunoassay demonstrates high sensitivity for the IV/A with a limit of detection (LOD) as low as 32.37 fg mL^{-1} and 54.97 fg mL^{-1} in buffer and serum, respectively. For the practical need, a clinically isolated IV/A/H3N2 and spike protein of SARS-CoV-2 were detected with the LODs of 17 pfu mL^{-1} and 143 fg mL^{-1}, respectively. These results show the applicability of advanced TMB-NPs@PLGA-based colorimetric sensor for highly sensitive detection of the airborne respiratory virus.

Introduction

In the last decade, immunoassay development has been progressing majorly centering on the signal amplification to boost its sensitivity and highly selective signal to the target bio-analytes.[1–3] The signal measurement used in biosensors is majorly based on colorimetric, fluorescent, and chemiluminescence. The primary drawback of the fluorescent and chemiluminescence principle is physical quenching due to fluorescent dye interaction to the polymeric component and the requirement of instrument measurement. In the term of simplicity, the colorimetric detection is favorable for the naked eye analysis. However, it is difficult to precisely differ little change of the small amount of analyte owing to the low sensitivity[2, 4, 5] due to the intrinsic limitation of the enzymes.[6, 7] To overcome these issues while retaining the original advantages, an improved ELISA utilizing enzyme-loaded nanomaterial,[8, 9] or nanomaterial with peroxidase-like activity with high sensitivity, attracts significant interest.[10–13]

Up to recently, nanozyme is being pursued intensively and experienced rapid expansion in various fields and mechanism studies. However, the nanozymes' activity and specificity to the substrate are not attained to the enzyme's sophistication level.[14] Taking it to further mileage in an immunoassay for low concentration analytes, the limitation of the conjugated nanozyme on individually conjugated to antibodies lowered the usability to achieve highly sensitive detection and its practical need. The approach in constructing the signal amplification in an immunoassay is being shifted toward the strategy to increase the availability of the nanozyme in the single antibody-antigen binding. Several studies have been done to extravagate the signal by facilitating the immunosorbent vesicle-containing nanozyme[15, 16] or in situ seed growth of the nanozyme.[11, 17, 18] This showed escalating detection signal up to a certain degree of amplification, but the drawback on its simplicity needs to be reconsidered.

Recently, the research in an immunoassay is being shifted from enzyme-dependent to signal-dependent, pivoting on the signal molecules' amount corresponding to the antibody-antigen binding. Miao et al.[19] and Ren et al.[20] reported the hydrophobic interaction of curcumin on MoS_2 and π-stacking interaction of thymolphthalein and metal-organic framework (MOF)-polydopamine, respectively, both as signal molecule nanocarriers. These interactions are possibly loosened, leading to leakage of free signal molecules from the nanomaterials. In the signal amplification platforms of biosensors, liposomes are being used as the nano-encapsulation due to its intrinsic hydrophilic and hydrophobic head-and-tail monomer leading to self-assembly encapsulation.[16, 21] However, the ratio-dependent and its instability limited its practical use in storage and

† Equal contribution.
1. Department of Bioscience, Graduate School of Science and Technology, Shizuoka University, 836 Ohya Suruga-ku, Shizuoka 422-8529, Japan
2. Research Institute of Green Science and Technology, Shizuoka University, 836 Ohya Suruga-ku, Shizuoka 422-8529, Japan
3. Department of Infectious Diseases, Hamamatsu University School of Medicine, 1-20-1 Higashi-ku, Handa-yama, Hamamatsu 431-3192, Japan

*Corresponding author., Research Institute of Green Science and Technology, Shizuoka University, 836 Ohya, Suruga-ku, Shizuoka 422-8529, Japan.
E-mail address: park.enoch@shizuoka.ac.jp (E.Y. Park). Tel (Fax): +81-54-238-4887

its integrity against the physical and chemical conditions.[20, 22] In our previous work, the liposome encapsulation either using water-soluble nanozyme hindered the detection of low virus concentration because of the low species incorporation in the liposomal encapsulation in both organic and aqueous phase.[16] Polymeric encapsulation or nanovesicles in the nanostructure fabrication comprises the proteins or drugs as the core inside and enveloped by a typical polymeric membrane.[23] Among the polymeric biomaterials, poly(lactide-co-glycolide) (PLGA) is successfully implemented in numerous drug delivery formulations due to its synthetic malleability and biocompatibility. Benefited by the rich-carboxylic structure, PLGA can be easily conjugated to biomolecules.[24, 25] The coupled ligands, such as antibodies conjugated to the surface, could selectively recognize specific antigens that enable the nanovesicle's utilization for biosensor application.

In this work, the chromogen substrate, 3,3',5,5'-Tetramethylbenzidine (TMB), is introduced to the biosensor by being carried within PLGA encapsulation (TMB-NPs@PLGA). The signal amplification strategy centralized in the enrichment of signal molecules in a single nanovesicle with preceding co-precipitation. TMB-NPs@PLGA are conjugated to antibodies and bounded to the captured virus in the microtiter wells. Upon the addition of dimethyl sulfoxide (DMSO), the encapsulated TMB-NPs are released, dissolving the PLGA shell. Simultaneously, the TMB-NPs are also dissolved in the DMSO solution into TMB molecules. The TMB is then catalytically oxidized by self-assembled copper nanoflowers (CuNFs) and H_2O_2, developing intense blue color as the indicator for a virus's presence. The released many encapsulated TMB-NPs from the captured TMB-NPs@PLGA nanovesicles, even at low virus concentration, significantly amplify the colorimetric signal in the quantity of the oxidized TMB. The developed ultrasensitive colorimetric biosensor illustrates its ability to detect respiratory-infecting viruses, such as influenza virus (IV) and Spike protein of SARS-CoV-2 in a broad range with low detection limit femtogram level attributing to its profound architecture, easy manipulation, and facile storing of TMB-NPs.

Experimental Section

Materials and chemicals

$CuSO_4 \cdot 5H_2O$, ethyl acetate, DMSO, polyvinyl alcohol n=1500~1800, TMB were purchased from Dojindo (Osaka, Japan). bovine serum albumin (BSA) and H_2O_2 were purchased from Wako Pure Chem Inc. (Osaka, Japan). N-hydroxysuccinimide (NHS), N-(3-dimethylaminopropyl)-N'-ethylcarbodiimide hydrochloride (EDC) were obtained from Sigma-Aldrich Co. (St Louis, MO, USA). IV/A/Hongkong/H1N1 was obtained from ProSpec-Tany Technogene, Ltd. (East Brunswick, NJ, USA). Recombinant 2019-nCov Spike protein (RBD) (ABL-1-113) and anti-2019-nCov S Protein (RBD) monoclonal antibody (ABN9306) were purchased from Abvigen Inc. (Newark, NJ, USA). Biological agents are described in the Electronic Supplementary Information.

Preparation of TMB-NPs and TMB-NPs-encapsulated PLGA

To increase the small hydrophobic chromogen's water dispersity, such as TMB, the molecules were assembled into nanoparticles (NPs) because of the sudden change in the solvent environment. TMB solution in DMSO (10 mg mL^{-1}) was added into aqueous solution to form precipitation with BSA (1 mg mL^{-1}, w/v) in 10 mM PBS (pH 6.5). The mixture was continuously stirred for 12 h at 4°C, stabilizing the dispersed TMB-NPs formation. The turbid solution was then centrifuged and washed three times with PBS, followed by freeze-drying for further usage.

TMB-NPs re-dispersed in DI water were encapsulated in a double emulsion system of PLGA nanovesicles using the previously reported preparation with minor modifications.[25] Four hundred microliter of the aqueous solution of TMB-NPs was added to 2 mL of ethyl acetate, and 100 mg PLGA and the mixture was gently stirred with alternating sonication. After two minutes of emulsifying, the PLGA/TMB-NPs, 8 mL of polyvinyl alcohol (5%, w/w, aqueous) were added to the w/o emulsion to form a w/o/w double emulsion and stirred further for 5 min. To solidify the nanoparticles, the organic solvent was extracted by stirring the double emulsion with 200 mL of an aqueous solution of polyvinyl alcohol 0.1% (w/w) for 5 min. The resulting dispersion of nanoparticles was centrifuged at 15,000 g for 15 min and freeze-dried for further use.

Characterizations

Scanning electron microscopy (SEM) images were obtained using a scanning electron microscope (SEM, JSM-6510LV, JEOL, Japan). Transmission electron microscopy (TEM, JEM-2100F, JEOL, Ltd., Japan), powder X-ray diffraction (PXRD, RINT ULTIMA XRD, Rigaku Co., Japan), and UV–Vis absorption spectra measurements (UV-1800, Shimadzu, Kyoto, Japan) were performed as described in our previous work.[2, 16]

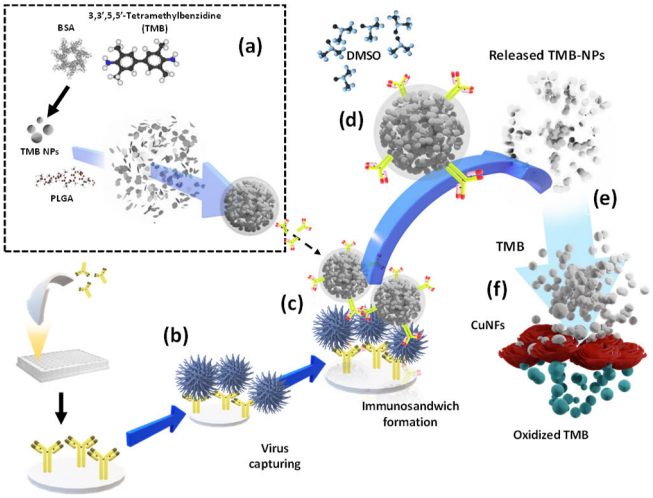

Scheme 1. The schematic illustration of the TMB-NPs@PLGA-based signal amplification platform. (a) The preparation of TMB-NPs@PLGA; (b) viruses are captured by the capture probe; (c) immunosandwich structured nanoconjugate with TMB-NPs@PLGA in the presence of virus; (d) addition of DMSO and the dissolving of the PLGA nanovesicle; (e) the release of TMB-NPs due to the dissolving of TMB-NPs by DMSO, and (f) the catalytic oxidation of TMB by CuNFs/H_2O_2 for colorimetric detection.

Detection of IV/A/H1N1 and clinically isolated IV/A/H3N2

Briefly, different concentrations of the target virus, IV/H1N1 was added into the wells containing capturing anti-hemagglutinin (HA)

antibody (anti-HA Ab) under the optimized amount at 100 ng (**Fig. S1a**) and blocking agent, 5% bovine serum albumin. The incubation of antibody-virus binding is optimized up to 1 h (**Fig. S1b**). After washing with PBS-0.1%Tween-20, 100 µL of anti-HA Ab-TMB-NPS@PLGA complex was added into the wells and incubated for an additional 1 h. The captured IV/A/H1N1 was bound to the anti-HA Ab-TMB-NPs@PLGA, and the immunocomplex sandwich was formed.

The wells were washed, and after the separation, 50 µL of the DMSO solution was added to disrupt the PLGA nanovesicles and release the encapsulated TMB-NPs. One hundred microliters of prepared substrate solution (H_2O_2 and CuNFs) were added to the wells, and blue color developed rapidly. After 5 min, 10% H_2SO_4 was added to stop the reaction, resulting in changing the blue color to yellow, followed by the absorbance measurement. Clinically isolated IV/A/Yokohama/110/2009/H3N2 and the spike protein of SARS-CoV-2 was applied following the same protocol using virus-specific antibody-conjugated TMB-NPs@PLGA for confirming the versatility of the assay system. For the specificity of the developed immunoassay, six control experiments were performed: 100 pg m^{-1} of hepatitis E virus-like particles (HEV-LPs) and norovirus-like particles (NoV-LPs), 10^4 copies mL^{-1} of white spot syndrome virus (WSSV), 10^3 pfu mL^{-1} of Zika virus, 20 µg mL^{-1} of norovirus (NoV) and mixture all the viruses.

Results and Discussion

Working principle of encapsulation of TMB-NPs for virus detection

The working principle of the developed TMB-NPs@PLGA-based colorimetric sensing method for ultrasensitive detection of IV/A/H1N1 is shown in **Scheme 1**. It comprises of TMB-NPs-encapsulated PLGA nanovesicles (TMB-NPs@PLGA), which are collective self-assembled TMB molecules and BSA inside PLGA nanovesicles **(Scheme 1a)**. Initially, the anti-HA Ab is immobilized in the microtiter plate wells via hydrophobic interaction to the polystyrene of the microplate. Different concentrations of the target IV/A are added to the anti-HA Ab immobilized wells **(Scheme 1b)**. Further, anti-HA Ab-conjugated TMB-NPs@PLGA are added to the wells allowing the formation of an immunocomplex sandwich structure. Anti-HA Ab-conjugated TMB-NPs@PLGA and anti-HA Ab formed sandwich-like structure with IV/A as depicted in **Scheme 1c**. After incubation, the wells are washed with PBS to remove the excess reagents and unbound anti-HA Ab-conjugated TMB-NPs@PLGA. After that, the successfully separated TMB-NPs@PLGA sandwich nanoconjugates in the wells are treated with DMSO to dissolve the PLGA membrane and release the encapsulated TMB-NPs **(Scheme 1d)**. The dissolving of the TMB-NPs@PLGA represents the first step of releasing the signal molecules in the system.

Additionally, the released TMB-NPs are also dissolved by the DMSO solution, acquiring highly concentrated TMB in the solution **(Scheme 1e)**, marking the second step of presenting the signal molecules in the system. The mixture of self-assembled CuNFs as peroxidase-mimicking nanomaterials and H_2O_2 solution are added to the wells for facilitating the catalytic oxidation of released TMB **(Scheme 1f),** exhibiting the color signals as proportional to quantification of the captured virus. In the absence of the target virus, the immunocomplex sandwich structure between TMB-NPs@PLGA and the bounded virus will not form. Without the TMB-NPs@PLGA in the system, there is an absence of TMB to be oxidized by CuNFs and H_2O_2 mixture for generating a colorimetric signal.

Characterization of the TMB-NPs, TMB-NPs@PLGA, and self-assembled CuNFs

The molecular self-assembly technique for the nanoparticles' preparation is evolving as a promising strategy to integrate different components for synthesizing desired hybrid nanomaterials spontaneously. The synthesis of TMB-NPs encapsulated within TMB-NPs@PLGA involves two steps, as illustrated in **Fig. 1a** and **b**: a) synthesis of TMB-NPs and b) encapsulation of synthesized TMB-NPs inside PLGA nanovesicles. The preparation commences with the self-assembly of TMB molecules using BSA as a template[26] with excellent dispersibility. The TEM image of the synthesized TMB-NPs is shown in **Fig. 1c.** The synthesized TMB-NPs are roughly circular with an average diameter of about 50 nm (**Fig. 1d**), showing electron density of TMB within the BSA aggregation. The TMB-NPs encapsulated PLGA nanovesicles (TMB-NPs@PLGA) are synthesized using the modified double emulsion solvent diffusion method. The formation of TMB-NPs@PLGA is verified using TEM (**Fig. 1e and f**). TMB-NPs@PLGA have presented in the form of collective TMB-NPs clustering together with a diameter of around 200 nm. The TEM image confirms the encapsulation of TMB-NPs in the PLGA nanovesicle (**Fig. 1f**), which clearly shows TMB-NPs are agglomerating, as the incorporation of TMB-NPs inside the PLGA nanovesicles with no sign of aggregation. **Fig. 1g** shows the digital photographs of TMB derived biomaterial dispersibility. TMB molecules were dissolved in an aqueous solution resulting in a light yellowish-white precipitate.

In contrast, TMB and BSA can be completely dissolved in DMSO and PBS, respectively, forming a clear solution. Accordingly, the self-assembled TMB-NPs are uniformly dispersed in PBS, attributing to the better aqueous dispersibility obtained from BSA's intrinsic hydrophilic property. TMB-NPs@PLGA are also found to maintain its uniformly dispersible in PBS as TMB-NPs attributing to free carboxyl groups from lactic acid of PLGA on the surface of TMB-NPs@PLGA.

Inspired by the unique features of protein-inorganic hybrid nanoflowers through self-assembly, the BSA-$Cu_3(PO_4)_2{\cdot}3H_2O$ hybrid nanoflower (CuNFs) were prepared. SEM image in **Fig. 1h** shows the flower-like structures of CuNFs with an average size of 400 – 500 nm, which have hierarchical structures with high surface-to-volume ratios. The TEM image of CuNFs (**Fig. 1i**) clearly shows the uniformly dispersed CuNFs attributing to the loaded hydrophilic BSA molecules. To confirm the structural properties of the CuNFs, XRD analysis is further performed. The XRD patterns of CuNFs (**Fig. S2** of Electronic Supplementary Information) are in good agreement with the JCPDS card (00-022-0548)[27, 28] indicating that CuNFs crystals are mainly composed of $Cu_3(PO_4)_2{\cdot}3H_2O$ crystals.

Catalytic activity of self-assembled CuNFs

TMB-NPs are successfully encapsulated inside the PLGA nanovesicles. As the subject of the utilization in immunoassay sensing, these encapsulated TMB-NPs need to be released to exhibit the detection signal required for virus detection. **Fig. 2a** shows the

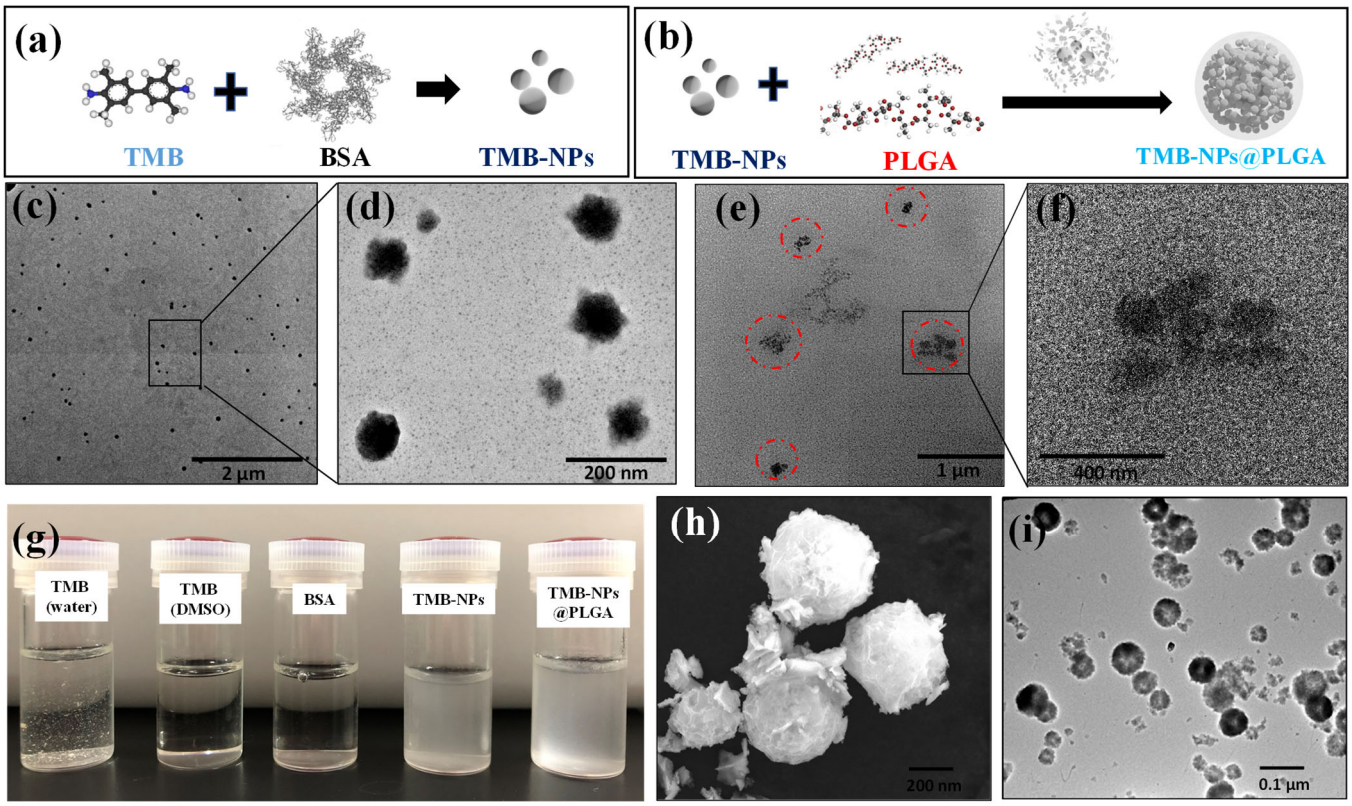

Fig. 1. The morphology characterization of TMB-NPs and TMB-NPs@PLGA. (a) and (b) show the schematic illustration of TMB-NPs and TMB-NPs@PLGA formation. (c)–(d) and (e)–(f) show TEM images of TMB-NPs and TMB-NPs@PLGA respectively; (g) shows the solution visualization of TMB solution, BSA solution, TMB-NPs, and TMB-NPs@PLGA; (h) and (i) shows the by SEM and TEM images of CuNFs.

schematic illustration of the release of TMB-NPs in the presence of water or DMSO. These released TMB-NPs are incubated with H_2O_2 and CuNFs. As shown in **Fig. 2b** and **c**, there is no occurrence of the developed color in the absence of the H_2O_2 as the co-substrate, the CuNFs as the nanozyme, or the DMSO as the releasing agent. The blue color changes to yellow after adding the acid solution to stop the TMB oxidation reaction (**Fig. 2c**). The absorbance of the developed color is shown in **Fig. 2d**, indicating a single peak in the presence of all components of the assay and the stability of TMB as signal molecules in the encapsulation and dissolving-and-releasing process. Also, the TMB-NPs and TMB-NPs@PLGA are assayed before and after the addition of DMSO. The digital photograph illustrates the difference of TMB-NPs with and without nanoencapsulation of PLGA. It shows a well-dispersed partially transparent solution to TMB-NPs@PLGA in the absence of DMSO (**Fig. 2e**). Opposite to its counterpart, TMB-NPs without the PLGA nanovesicle develop a slightly yellowish color with a partially white cloudy solution in the presence of H_2O_2/CuNFs in acidic conditions. These show desirable spatial protection on the TMB-NPs by the PLGA nanovesicle, isolating the TMB-NPs from external stimuli. In DMSO's presence, the higher catalytic oxidation of TMB is occurred on both TMB-NPs and TMB-NPs@PLGA, pointing out the dissolving-and-release mechanism of TMB-NPs@PLGA. DMSO dissolves the nanovesicles and follows up with the dissolving of TMB-NPs, releasing the TMB molecules to the H_2O_2/CuNFs solution.

The apparent steady-state kinetic parameters are examined to determine the catalytic activity of self-assembled CuNFs. By keeping the constant concentration of the respective co-substrate, the experiments are performed with various concentrations of substrate and a fixed concentration of co-substrate. Referring to the typical Michaelis-Menten kinetics, the Lineweaver-Burk double reciprocal plot is generated. The reaction velocity as the function of the respective concentration of the substrate is plotted. It shows excellent linearity indicating the intrinsic properties of CuNFs as nanozyme (inset of **Fig. 2f and g**). As listed in **Table S1**, the K_m value (mM) and maximal velocity (v_{max}) of CuNFs for both substrates were determined based on the Michelin-Menten graph. The K_m values of CuNFs and HRP to TMB are 0.07 mM and 0.43 mM, respectively. It shows CuNFs exhibit a lower K_m value than horseradish peroxidase (HRP), indicating a higher affinity of the nanozyme to the TMB substrate. Besides, the v_{max} of CuNFs is 0.12 μM/s for TMB and 0.02 μM/s for H_2O_2. The CuNFs possess a high surface area and essential electrostatic interaction to the favorable TMB substrate and H_2O_2, which allow a considerably sufficient peroxidase-like activity fulfilling the prerequisite to develop sensitive nanozyme-based colorimetric immunoassay.

Further, the catalytic activity of CuNFs with optimum concentration at 50 μg mL^{-1} (**Fig. S1c**) has compared to copper (Cu) ions for the beneficial utilization in virus detection in the presence of 0.5 M H_2O_2 (**Fig. S1d**). Based on the initial concentration of CuNFs precursor, 10 mM Cu ions are assayed against the catalytic properties of the CuNFs in the influenza virus detection. Using Cu ions only, the signal is compared to catalytic CuNFs (**Fig. 3a**) in the low concentration of the influenza virus. In the nanogram level of the

influenza virus, the signal by Cu ions is generated down to 50% compared to the CuNFs. The advantage of utilizing the nanozyme implicates the crystalline structure of the copper-phosphate and its catalytic properties of the nanoflower for a better signal generation with a lower baseline signal.

Optimization of TMB-NPs encapsulation in TMB-NPs@PLGA

In this work, the significant points for the signal amplification strategy for immunoassay purposes are the maximal encapsulation of TMB-NPs inside the PLGA nanovesicles and the reaction time required to develop the color change. Firstly, the loading amount of TMB-NPs is optimized to achieve maximal encapsulation inside the PLGA nanovesicles. The as-prepared TMB-NPs solutions of 25, 50, 75, and 100 mg mL^{-1} are used for the PLGA encapsulation with 0 mg mL^{-1} representing empty PLGA nanovesicle. As shown in **Fig. 3b**, it is evident that the absorbance signal continuously increased along with the increasing concentrations of TMB-NPs, attributing to the increase of TMB-NPs concentration in the presence of CuNFs and H_2O_2. To optimize the encapsulated number of TMB-NPs in the PLGA nanovesicles, the assay is performed using various concentrations of TMB-NPs encapsulated in PLGA nanovesicles with and without the DMSO. It can be seen that there is no signal amplification with and without the addition of DMSO in empty PLGA nanovesicles, showing the TMB signal solely in the form of TMB-NPs. Comparing the signal generated before and after the DMSO addition, 75 mg mL^{-1} is determined as the optimal loading concentration in the PLGA nanovesicles.

Further, based on the absorbance value, the corresponding TMB molecules' concentration is calculated corresponding to its molar absorption coefficient. The catalytic oxidized TMB molecules' concentration is estimated at 43.1 mg mL^{-1}, which indicates the loading capacity of the PLGA nanovesicle is up to 53.4%. The change of absorbance upon the release of TMB-NPs from PLGA nanovesicles synthesized using 100 mg mL^{-1} is relatively similar to 75 mg mL^{-1}. The difference in absorbance intensity before and after the release of TMB-NPs upon the addition of DMSO expressed in the change of absorbance is highly desirable for obtaining sensitive and reliable detection. Therefore, TMB-NPs@PLGA nanovesicles, which are synthesized using 75 mg mL^{-1} of TMB-NPs solution, are used to prepare TMB-NPs@PLGA in further experiments.

Fig. 3c shows the incubation time as the function of the absorbance change in the mixture of TMB-NPs@PLGA and CuNFs/H_2O_2 with and without DMSO. Before the optimization, the TMB-NPs@PLGA was reacted with only H_2O_2. Low absorbance was shown due to no involvement of the catalytic reaction by CuNFs and grounding the need of the CuNFs as a nanozyme. Although there is an increase in the absorbance response compared to the only H_2O_2, a slight change of absorbance is observed in TMB-NPs@PLGA incubated with CuNFs/H_2O_2.

In contrast, the absorbance is noticeably and gradually increasing after DMSO's addition and incubation of TMB-NPs@PLGA with CuNF/H_2O_2. The absorbance increases rapidly from 0 to 100 sec of the incubation time, and the stationary absorbance intensity is observed after 120 sec. There is a provision period to maximize the signal, mainly laid on the equilibrium of the redox reaction between the TMB/H_2O_2 system and CuNFs. After the equilibrium, the absorbance is constant until 200 sec. Therefore, the reaction time for developing the color is optimized to be 120 sec in the developed colorimetric immunoassay for virus detection.

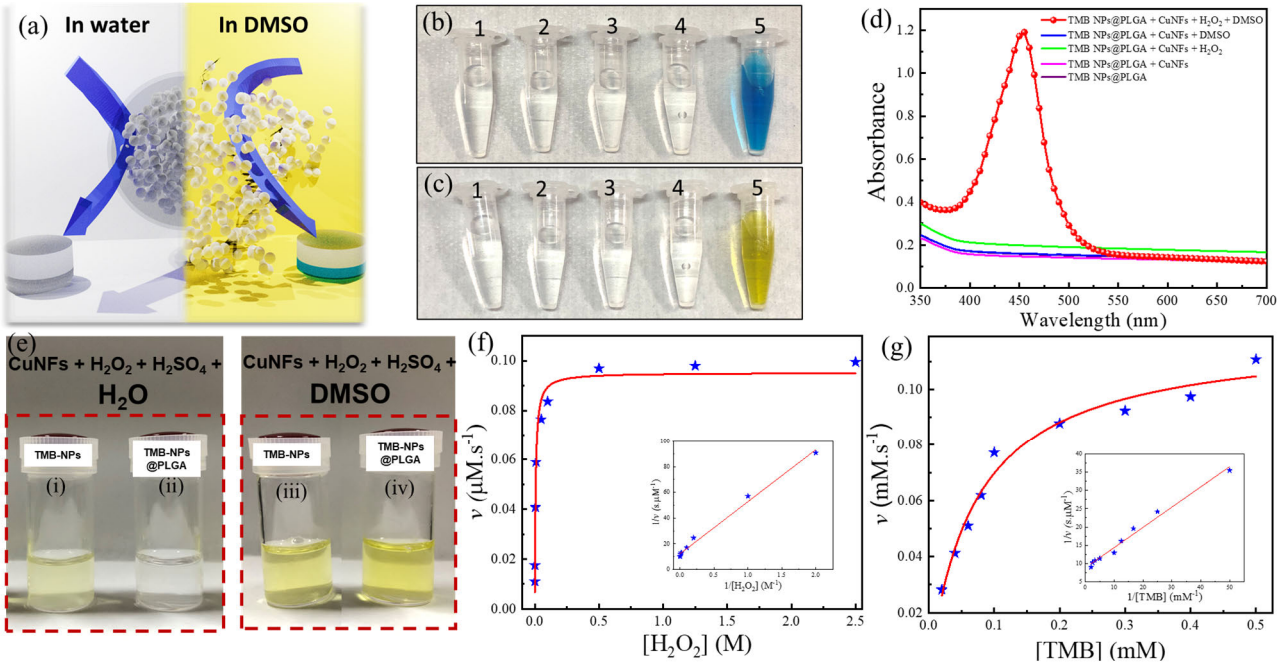

Fig. 2. (a) The schematic illustration of the DMSO as the releasing agent of the dissolving of TMB-NPs@PLGA; (b) and (c) demonstrate the color change of TMB-NPs@PLGA in the presence of DMSO, H_2O_2, and CuNFs for before and after acid addition respectively. (1) TMB-NPs@PLGA, (2) TMB-NPs@PLGA + CuNFs, (3) TMB-NPs@PLGA + CuNFs + H_2O_2, (4) TMB-NPs@PLGA + CuNFs + DMSO, and (5) TMB-NPs@PLGA + DMSO + CuNFs + H_2O_2. (d) The corresponding absorbance spectrum of the illustration (c) of the catalytic oxidation of TMB-NPs@PLGA; (e) represents the color change of TMB-NPs (i, iii) and TMB-NPs@PLGA (ii, iv) in H_2O (i, ii) and DMSO (iii, iv); and (f) and (g) show the Michelin-Menten plot of steady-state kinetic of CuNFs toward H_2O_2 and TMB, respectively (The inset showed the linearity of LB plot).

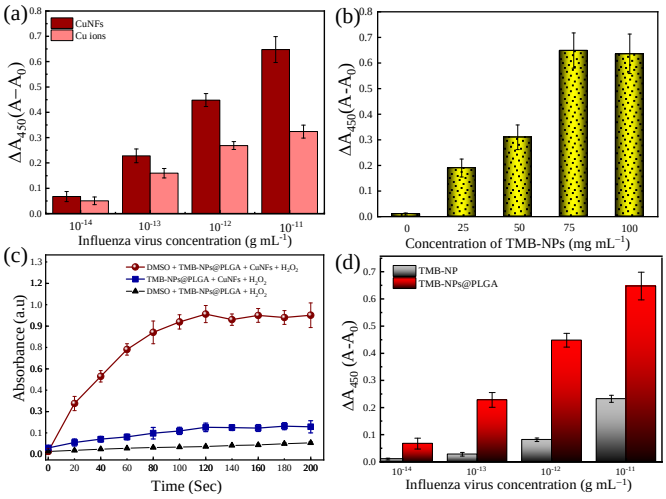

Fig. 3. (a) Comparison of catalytic activity of CuNFs and Cu ions in H_2O_2/TMB system for various concentrations of IV; the optimization of the TMB-NPs@PLGA corresponding to the encapsulation amounts of TMB-NPs in PLGA nanovesicles (b) and the incubation time for the change in absorbance intensity of TMB-NPs, CuNFs, and H_2O_2 mixture (c); (d) comparison of IV/A detection using TMB-NPs@PLGA and TMB-NPs. A_0 and A indicate the absorbance before and after the addition of DMSO, respectively. The error bars indicate the SD of the triple measurement.

Analytical performance of the sensing system

To achieve a highly sensitive detection limit, the main point weighted heavily is the nanoparticles encapsulation-based signal amplification strategy in this developed colorimetric immunoassay. First, to underline the advantage of the encapsulation of TMB-NPs inside the PLGA nanovesicles in amplifying the signal, the bare TMB-NPs, which are self-assembled with anti-HA Ab and BSA, are used instead of TMB-NPs@PLGA for detecting IV/A. Hypothetically, the TMB-NP can demonstrate a color signal for IV/A detection similar to the TMB-NPs@PLGA. Based on antigen-antibody interaction, a sole immunocomplex can only be abutted with a single TMB-NP. In contrast, the encapsulation of TMB helps localization of the signal substrate and enriches the signal generation for individual antibody-antigen binding. The IV detection immunoassay using bare TMB-NPs and TMB-NPs@PLGA is shown in **Fig. 3d**. Interpreting the difference in the absorbance signal, utilizing the TMB-NPs@PLGA improved 100-fold higher detection sensitivity compared to only TMB-NPs. The encapsulation of the TMB-NPs localizes a higher concentration of TMB molecules even at a low concentration of the virus up to 3.5-folds of localized concentration of the colorimetric signal.

Besides the encapsulation of the signal molecules, in the juxtapose to our previous work[11, 29] using electrostatic interaction as the conjugation force, the antibodies' chemically-conjugation on the nanovesicles upholds the increase of the antibody-antigen by preventing the random confirmation on the antibodies. Moreover, the PLGA nanovesicles provide the conjugation site; instead of the TMB-NPs, the reactivity and morphology of the NPs are well-preserved within the PLGA nanovesicles. Lastly, TMB molecules' encapsulation instead of the nanozyme like noble metals or metal oxides nanoparticles[15, 16] shows more effective signal generation. The catalytic oxidation of the TMB molecules as the determining factor is reflected in the low value of the K_m of the CuNFs. Subjection to the low detection limit, the collective TMB molecules' reactiveness in the form of NPs within the PLGA nanovesicles is essential for amplifying the signal in immunoassay format.

Adopting a typical immunosorbent assay, the colorimetric immunoassay is applied to the increasing concentration of IV/A/H1N1. The corresponding result of blue color shows a gradient pattern from low to intense blue color and changed proportionally to yellow color after the reaction is stopped. The measured absorbance at 450 nm (with 650 nm as the reference absorbance) increased as the function of the concentration of IV/A/H1N1 (**Fig. 4a**). The calibration line with a correlation coefficient (R^2) of 0.983 was obtained with satisfactory linearity from 101–106 fg mL^{-1}. Also, the limit of detection (LOD) is 32.37 fg mL^{-1}, which is determined by based on the equation 3.3σ-c/S,[30] in which c, S and σ represent the y-intercept and the gradient slope of the calibration line and the standard deviation of the blank signal, respectively. The low LOD can be attributed to two contributing factors: the presence of optimized nanozyme concentration and highly localized TMB molecules in low antibody-antigen conjugation, inclining the increase in the slope of the detection and generating a signal in the low quantity of immuno-conjugation.

To establish a reliable and practical immunoassay, a dilution series of concentrations of IV/A/H1N1 is spiked in the biological human serum matrix. The developed colorimetric immunoassay shows a linear increase of absorbance to the function of the introduced virus in the medium. **Fig. S3** in Electronic Supplementary Information shows the calibration line for IV/A/H1N1 detection using 10% human serum as a detection medium. The gradient of the calibration line is slightly flat shifted than the linear calibration from the IV detection in buffer solution up to 15%. However, the responsive linearity

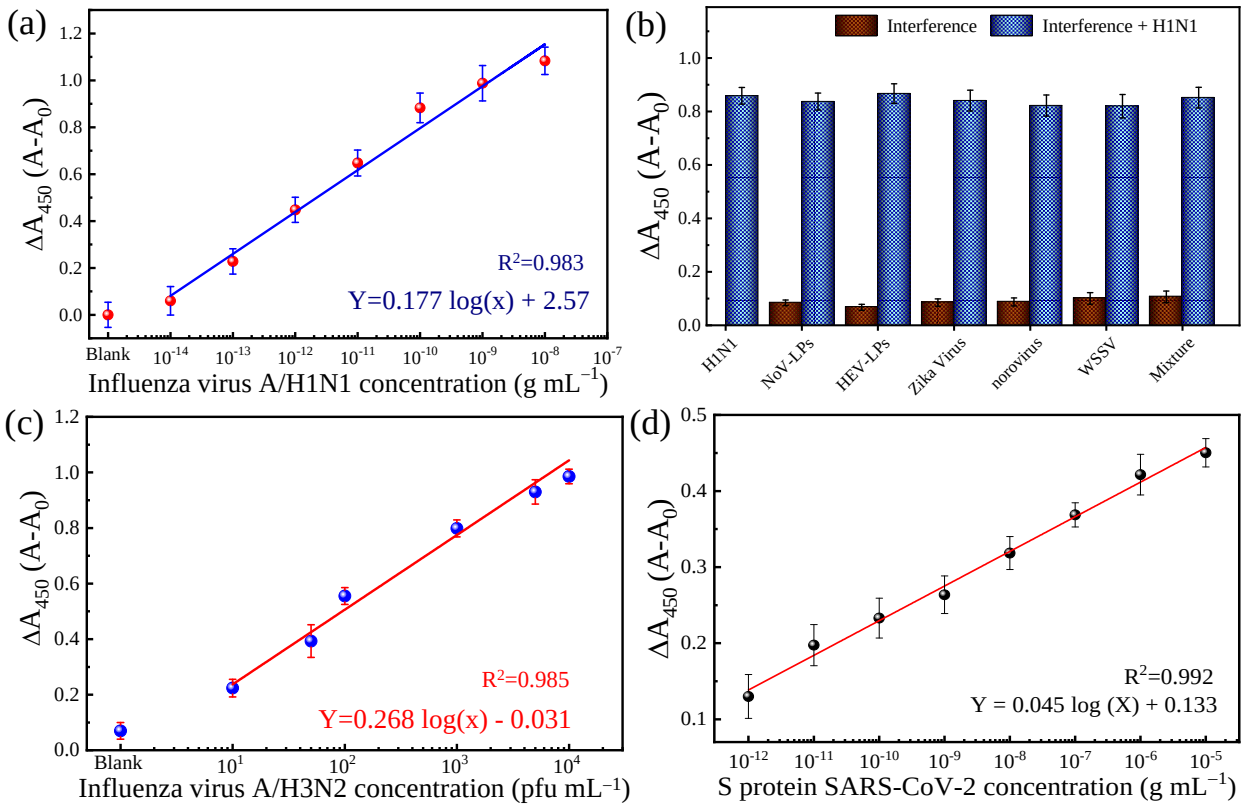

Fig. 4. (a) The calibration line of the detection of IV/A/H1N1 by TMB-NPs@PLGA based colorimetric detection in PBS system; (b) the selectivity test in the presence of interferences. The calibration curve obtained using the clinically isolated IV/A/H3N2 (c) and recombinant spike protein of SARS-CoV-2 (d). A_0 indicates the absorbance of a blank sample. The error bars represent the standard deviation of the three measurements

.

of the IV detection confirmed the applicability of the developed colorimetric immunoassay in a sophisticated serum matrix. Prompt to the matrix effect, the slope of the calibration curve is flattened, resulting in an increase of the LOD value to 54.97 fg mL^{-1}, which is comparable to previously reported works for its real application (**Table S2**).[31–34]

Specificity of TMB-NPs@PLGA-based immunoassay

The selectivity of the developed TMB-NPs@PLGA based colorimetric immunoassay for IV/A/H1N1 detection is evaluated. The dsDNA virus WSSV; the recombinant expressed NoV-LPs and HEV-LPs; and the RNA virus, Zika virus, and NoV are assayed as interferences (negative analytes) to examine the anti-interference effect and the selectivity of the developed TMB-NPs@PLGA-based immunoassay, which is collated to the response of IV/A/H1N1. **Fig. 4b** shows the change in absorbance intensity of developed immunoassay to the mixture of negative analytes and IV/A/H1N1. The intense color developed in the presence of IV/A/H1N1 in the samples, but not in the negative samples containing interferences only. The interfering viruses are unrecognizable by the capturing antibodies and anti-HA antibodies on the conjugated TMB-NPs@PLGA, which are specific to IV/A. As a result, after washing, there is no TMB-NPs@PLGA in the reaction chamber, resulting in no TMB molecules even after the addition of DMSO, the only small increase in the absorbance intensity in the detection of the negative samples justified the superior specificity of TMB-NPs@PLGA-based colorimetric immunoassay towards IV/A detection.

Detection of clinical-isolated IV/A/H3N2 and S-protein of SARS-CoV-2

To demonstrate the practicability of the TMB-NPs@PLGA-based colorimetric immunoassay, the clinically isolated samples containing IV/A/H3N2 are applied to the developed

immunoassay (**Fig. 4c**). The absorbance intensity increased continuously proportionally to the increasing concentration of IV/A/H3N2 from 101–104 pfu mL^{-1}, developing the proportional gradient of color (**Fig. S4**). The detection of the IV/A/H3N2 shows the R^2 value of 0.985 with the LOD of 17 pfu mL^{-1}. The developed immunoassay using the TMB-NPs@PLGA nanovesicles proffers a higher sensitivity than the available commercial IV detection kit (Quicknavi-Flu 2, Denka Seiken Co., Ltd. Tokyo, Japan) and the conventional ELISA using HRP and gold nanoparticles (**Table S3**)[31–32]. These results strongly demonstrate that our TMB-NPs@PLGA-based immunoassay possesses a strong anti-interference ability and highly sensitive for practical use.

In response to the recent outbreak of Covid-19, the TMB-NPs@PLGA-based immunoassay is applied to detect the spike protein of SARS-CoV-2. The spike protein is used as the antigen to demonstrate the direct coronavirus detection targeting the surface protein. As shown in **Fig. 4d**, the wide linearity from picogram to nanogram level is achieved with an excellent linear response depending on the concentration of the spike protein. The LOD is calculated down to 143 fg mL^{-1} with the R^2 value of 0.992, in which the femtogram level detection of the spike protein of SARS-CoV-2 agrees to other biosensors with higher complexity fabrication and analysis.[35–37]

Conclusions

In this study, we have prepared TMB-NPs-encapsulated PLGA nanovesicles using self-assembly and the nano-co-precipitation process. The TMB-NPs@PLGA nanovesicles serve as a signal amplification source for highly selective and sensitive detection of the IV/A. Self-assembly of TMB-NPs@PLGA integrated the dispersity of hydrophobic molecules by BSA and polymeric encapsulation. The bound TMB-NPs@PLGA recognizing the captured virus could be dissolved with DMSO, releasing the encapsulated TMB-NPs. Our results further successfully demonstrated the simultaneous dissolving of the PLGA nanovesicles and TMB-NPs, enriching the signal molecules in low antibody-antigen sandwich structure nanoconjugates. Released TMB-NPs produced amplified colorimetric signal upon oxidation by self-assembled CuNFs in the presence of H_2O_2. The developed immunoassay utilizing the TMB-NPs@PLGA nanovesicles and CuNFs nanozyme demonstrate the detection of the IV/A using the colorimetric signal readout in linear response from 10 fg level to 10 ng level with the LOD of 32 fg mL^{-1} and a linear range of 101 to 104 pfu mL^{-1} of clinically isolated IV/A/H3N2 with LOD of 17 pfu mL^{-1}. Further, the concentrated signal molecules nanovesicles in the immunoassay are adopted to target the spike protein of SARS-CoV-2, which shows femtogram level detection. The proposed immunoassay provides a reliable and easy-to-be-adapted ultrasensitive diagnostic platform to detect the various respiratory-infecting virus.

Acknowledgments

We would like to express our sincere thank you to Dr. Tian-Cheng Li of National Institute of Infectious Diseases, Dr. Jun Satoh of National Research Institute of Aquaculture of Japan Fisheries Research and Education Agency, Professor K. Morita of Institute of Tropical Medicine Nagasaki University, and Mr. F. Abe of Department of Microbiology, Shizuoka Institute of Environment and Hygiene for providing HEV-LP, WSSV, Zika virus, and NoV, respectively. ABG and IMK sincerely thank the Japan Society for the Promotion of Science (JSPS) for a postdoctoral fellowship (19F19064) and research fellowship-DC (20J22358), respectively.

Notes and references

1. A. D. Chowdhury, A. B. Ganganboina, Y.-c. Tsai, H.-c. Chiu and R.-a. Doong, *Analytica Chimica Acta*, 2018, **1027**, 109-120.
2. A. D. Chowdhury, A. B. Ganganboina, F. Nasrin, K. Takemura, R.-a. Doong, D. I. S. Utomo, J. Lee, I. M. Khoris and E. Y. Park, *Anal. Chem.*, 2018, **90**, 12464–12474.
3. A. B. Ganganboina and R.-a. Doong, *Microchim. Acta*, 2018, **185**, 526.
4. S. Oh, J. Kim, V. T. Tran, D. K. Lee, S. R. Ahmed, J. C. Hong, J. Lee, E. Y. Park, and J. Lee, *ACS Appl. Mater. Interfaces*, 2018, **10**, 12534−12543.
5. S. R. Ahmed, J. Kim, T. Suzuki, S. Neethirajan, J. Lee, and E. Y. Park, *Sci. Rep.*, 2017, **7**, 44495.
6. R. C. Murdock, L. Shen, D. K. Griffin, N. Kelley-Loughnane, I. Papautsky, and J. A. Hagen, *Anal. Chem.*, 2013, **85**, 11634−11642.
7. L. Yu, C. M. Li, Y. Liu, J. Gao, W. Wang and Y. Gan, *Lab Chip*, 2009, **9**, 1243−1247.
8. H. Lin, Y. Liu, J. Huo, A. Zhang, Y. Pan, H. Bai, Z. Jiao, T. Fang, X. Wang, and Y. Cai, *Anal. Chem.*, 2013, **85**, 6228−6232.
9. Y. Zhao, Y. Zheng, R. Kong, L. Xia, and F. Qu, *Biosens. Bioelectron.*, 2016, **75**, 383−388.
10. C. N. Loynachan, M. R. Thomas, E. R. Gray, D. A. Richards, J. Kim, B. S. Miller, J. C. Brookes, S. Agarwal, V. Chudasama and R. A. McKendry, *ACS Nano*, 2018, **12**, 279−288.
11. I. M. Khoris, A. D. Chowdhury, T.-C. Li, T. Suzuki, and E. Y. Park, *Anal. Chim. Acta*, 2020.
12. N. Cheng, Y. Song, M. M. Zeinhom, Y.-C. Chang, L. Sheng, H. Li, D. Du, L. Li, M.-J. Zhu and Y. Luo, *ACS Appl. Mater. Interfaces*, 2017, **9**, 40671−40680.
13. A. B. Ganganboina and R.-a. Doong, *Sensors, and Actuators B: Chemical*, 2018, **273**, 1179-1186.
14. Y. Zhou, B. Liu, R. Yang, and J. Liu, *Bioconjugate Chem.*, 2017, **28**, 2903−2909.
15. H. Ye, K. Yang, J. Tao, Y. Liu, Q. Zhang, S. Habibi, Z. Nie and X. Xia, *ACS Nano*, 2017, **11**, 2052−2059.
16. A. B. Ganganboina, A. D. Chowdhury, I. M. Khoris, F. Nasrin, K. Takemura, T. Hara, F. Abe, T. Suzuki and E. Y. Park, *Biosensors and Bioelectronics*, 2020, 112169.
17. S. Wang, Z. Chen, J. Choo and L. Chen, *Anal. Bioanal.Chem.*, 2016, **408**, 1015−1022.
18. I. M. Khoris, K. Takemura, J. Lee, T. Hara, F. Abe, T. Suzuki, and E. Y. Park, *Biosens. Bioelectron.*, 2019, **126**, 425−432.
19. L. Miao, C. Zhu, L. Jiao, H. Li, D. Du, Y. Lin and Q. Wei, *Anal. Chem.*, 2018, **90**, 1976−1982.
20. R. Ren, G. Cai, Z. Yu, Y. Zeng and D. Tang, *Anal. Chem.*, 2018, **90**, 11099−11105.
21. L. Sercombe, T. Veerati, F. Moheimani, S. Y. Wu, A. K. Sood, and S. Hua, *Front. Pharmacol.*, 2015, **6**, 286.

22. Y. Lin, Q. Zhou, Y. Zeng, and D. Tang, *Microchim. Acta*, 2018, **185**, 311.
23. U. Nagaich, *J. Adv. Pharm. Technol. Res.*, 2018, **9**, 65.
24. P. Kocbek, N. Obermajer, M. Cegnar, J. Kos, and J. Kristl, *J. Controlled Release*, 2007, **120**, 18−26.
25. Y. Zhang, H. Wang, S. Stewart, B. Jiang, W. Ou, G. Zhao and X. He, *Nano Lett.*, 2019, **19**, 9051−9061.
26. L. Jiao, H. Yan, W. Xu, Y. Wu, W. Gu, H. Li, D. Du, Y. Lin, and C. Zhu, *Anal. Chem.*, 2019, **91**, 8461−8465.
27. J. Ge, J. Lei, and R. N. Zare, *Nat. Nanotechnol.*, 2012, **7**, 428−432.
28. M. Li, M. Luo, F. Li, W. Wang, K. Liu, Q. Liu, Y. Wang, Z. Lu, and D. Wang, *The Journal of Physical Chemistry C*, 2016, **120**, 17348−17356.
29. S. R. Ahmed, J. Kim, T. Suzuki, J. Lee and E. Y. Park, *Biotechnol. Bioeng.*, 2016, **113**, 2298−2303.
30. A. B. Ganganboina and R.-A. Doong, *Scientific reports*, 2019, **9**, 1-11.
31. K. Takemura, O. Adegoke, N. Takahashi, T. Kato, T.-C. Li, N. Kitamoto, T. Tanaka, T. Suzuki and E. Y. Park, *Biosens. Bioelectron.*, 2017, **89**, 998−1005.
32. S. R. Ahmed, M. A. Hossain, J. Y. Park, S.-H. Kim, D. Lee, T. Suzuki, J. Lee, and E. Y. Park, *Biosens. Bioelectron.*, 2014, **58**, 33−39.
33. Y.-F. Chang, S.-F. Wang, J. C. Huang, L.-C. Su, L. Yao, Y.-C. Li, S.-C. Wu, Y.-M. A. Chen, J.-P. Hsieh and C. Chou, *Biosens. Bioelectron.*, 2010, **26**, 1068−1073.
34. U. Jarocka, R. Sawicka, A. Góra-Sochacka, A. Sirko, W. Zagórski-Ostoja, J. Radecki and H. Radecka, *Sensors*, 2014, **14**, 15714−15728.
35. G. Seo, G. Lee, M. J. Kim, S.-H. Baek, M. Choi, K. B. Ku, C.-S. Lee, S. Jun, D. Park, and H. G. Kim, *ACS Nano*, 2020, **14**, 5135–5142.
36. S. Mavrikou, G. Moschopoulou, V. Tsekouras, and S. Kintzios, *Sensors*, 2020, **20**, 3121.
37. G. Qiu, Z. Gai, Y. Tao, J. Schmitt, G. A. Kullak-Ublick and J. Wang, *ACS Nano*, 2020, **14**, 5268–5277.

Appendix A. Electronic Supplementary Information

Self-Assembled Chromogen-loaded Polymeric Cocoon for Respiratory Virus Detection

Indra Memdi Khoris[1,†], Akhilesh Babu Ganganboina[2,†], Tetsurou Suzuki[3], Enoch Y. Park [*,1,2]

† Equal contribution.
1. Department of Bioscience, Graduate School of Science and Technology, Shizuoka University, 836 Ohya Suruga-ku, Shizuoka 422-8529, Japan
2. Research Institute of Green Science and Technology, Shizuoka University, 836 Ohya Suruga-ku, Shizuoka 422-8529, Japan
3. Department of Infectious Diseases, Hamamatsu University School of Medicine, 1-20-1 Higashi-ku, Handa-yama, Hamamatsu 431-3192, Japan

**Corresponding author.*, Research Institute of Green Science and Technology, Shizuoka University, 836 Ohya, Suruga-ku, Shizuoka 422-8529, Japan.
E-mail address: park.enoch@shizuoka.ac.jp (E.Y. Park). Tel (Fax): +81-54-238-4887

Materials and methods

Biological agents

Anti-IV/A/H1, H2, and H3 (Anti-HA) and anti-IV/A/H3N2 antibodies (anti-IV/A/H3N2) were purchased from Sino Biological Inc. (Beijing, China). Clinically isolated IV/A/Yokohama/110/2009/H3N2 was kindly provided by Dr. C. Kawakami of the Yokohama City Institute of Health, Japan. The recombinant baculovirus expressed-Hepatitis E virus-like particles (HEV-LPs) were provided by Dr. Tian Chen-Li from National Institute of Infectious Disease Japan. Zika virus and white spot syndrome virus (WSSV) were provided by Prof. K. Morita of Institute of Tropical Medicine, Nagasaki University, and Dr. J. Satoh of National Research Institute of Aquaculture, Japan Fisheries Research, and Education Agency respectively. Norovirus (NoV) was kindly provided by Mr. F. Abe of Shizuoka Institute of Environmental and Hygiene, Shizuoka, Japan. Norovirus-like particle (NoV-LP) was expressed using a baculovirus expression system [1]. All experiments were conducted using deionized (DI) water.

Preparation of CuNFs.

Inspired by the protein inorganic hybrid nanoflowers, CuNFs, were prepared by a one-pot bio-mineralization process with some modifications[2, 3]. Typically, 100 μL of BSA (5 mg/mL) was dissolved into 10 mL of 1 × PBS (pH 7.4) for incubation of 0.5 h under slow stirring. Then, 400 μL of $CuSO_4 \cdot 5H_2O$ solution (120 mM) and 50 μL of 10% KCl solution were added to the BSA solution and further incubated for an additional 48 h. The obtained solution was centrifuged (6500 g, 15 min) at 7°C and washed three

times. Thus, obtained CuNFs were freeze-dried and stored at －20°C for further usage.

Catalytic activity of CuNFs.

CuNFs were analyzed for its peroxidase-like activity in the catalytic oxidation of TMB by H_2O_2 according to previously report[4] with some modification. The steady-state kinetic assay was carried out at room temperature on the CuNFs in the working solution, containing 40 mM TMB reagents and 500 mM H_2O_2 (1:4, v/v in DI water). The assays were performed in series of concentration of co-substrate to a fixed concentration of the substrate in the corresponding working solution. The absorbance of the developed color was measured at 653 nm using UV-Vis spectroscopy.

Preparation of Anti-IV/A/HA antibody-conjugated TMB-NPS@PLGA.

The conjugation of anti-HA antibody (Ab) or Anti-IV/A/H3N22 Ab to TMB-NPs@PLGA was done by EDC/NHS conjugation chemistry as described in our previous work [5].

Calculation of the Limit of Detection (LOD)

Based on the calibration curve of the developed assay, the LOD of the developed assay on the Influenza virus A/H1N1 and A/H3N2, and spike protein of SARS-CoV-2 were determined based on the y-intercept (c) and the gradient slope (S) of the calibration line and the standard deviation (σ) of the lowest detectable signal (blank), respectively.[6]

As the calibration curve is represented in semi-log graph, the corresponding LOD is defined as [LOD] = $e^{3.3\sigma/S}$.

$$Y = S \cdot \log(X) + c \quad (1)$$

$$Y_{LOD} = S \cdot \log(X_{LOD}) + c \quad (2)$$

Where Y_{LOD} denotes the absorbance value obtained from the lowest concentration of the virus sample by the developed assay. X_{LOD} indicates the lowest concentration of virus-containing sample which can be detectable by the developed assay.

As $Y_{LOD} \leq \Delta A_{Blank} + 3.3\sigma$ (3)

The ΔA_{Blank} is 0 as ΔAbs is represented with $A - A_{Blank}$.

From Eq. (2) and (3)

$$S \cdot \log(X_{LOD}) + c = 3.3\sigma \quad (4)$$

$$S \cdot \log(X_{LOD}) = 3.3\sigma - c \quad (5)$$

From Eq. (5), the X_{LOD} was defined as follow,

$$X_{LOD} \leq e^{\frac{3.3\,\sigma - c}{S}} \quad (6)$$

The illustration of the LOD calculation is shown in Fig. S5.

Table S1. The Kinetic Parameter of CuNFs in comparison to natural peroxidase

Catalyst	Substrate	K_m (mM)	v_{max} (μM/s)
CuNFs	TMB	0.07	0.12
CuNFs	H_2O_2	6.50	0.02
HRP	TMB[7]	0.43	0.10
HRP	H_2O_2[7]	3.70	0.09

Table S2. Comparison of Previous Work Related to IV/A Detection

Detection method	Strain of IV	LOD	Reference
LSPR-induced immunofluorescence	A/New Caledonia/20/99	0.09 pg/mL	8
Metal enhanced fluorescence	A/New Caledonia/20/99	1 ng/mL	9
Peroxidase-mimicking nanozyme	A/New Caledonia/20/99	10 pg/mL	10
LSPR fiber-optic	A/Vietnam/1203/ 2004	13.9 pg/mL	11
Electrochemical immunosensor	A/Poland/08/2006	2.2 pg/mL	12
Immunochromatography assay	A/California/12/2009	76.7 ng/mL	13
Nanovesicle based immunoassay	A/New Caledonia/20/99	0.05 pg/mL	(This work)

Table S3. Clinically Isolated IV/A/H3N2 Detection

	Virus Concentration (pfu/mL)						
Detection Method	5000	1000	100	50	25	10	1
Commercial IV detection kit	+	-	-	-	-	-	-
HRP-based ELISA[6, 8]	+	+	-	-	-	-	-
AuNPs-based Immunoassay[8]	+	+	+	+	-	-	-
This study	+	+	+	+	+	+	-

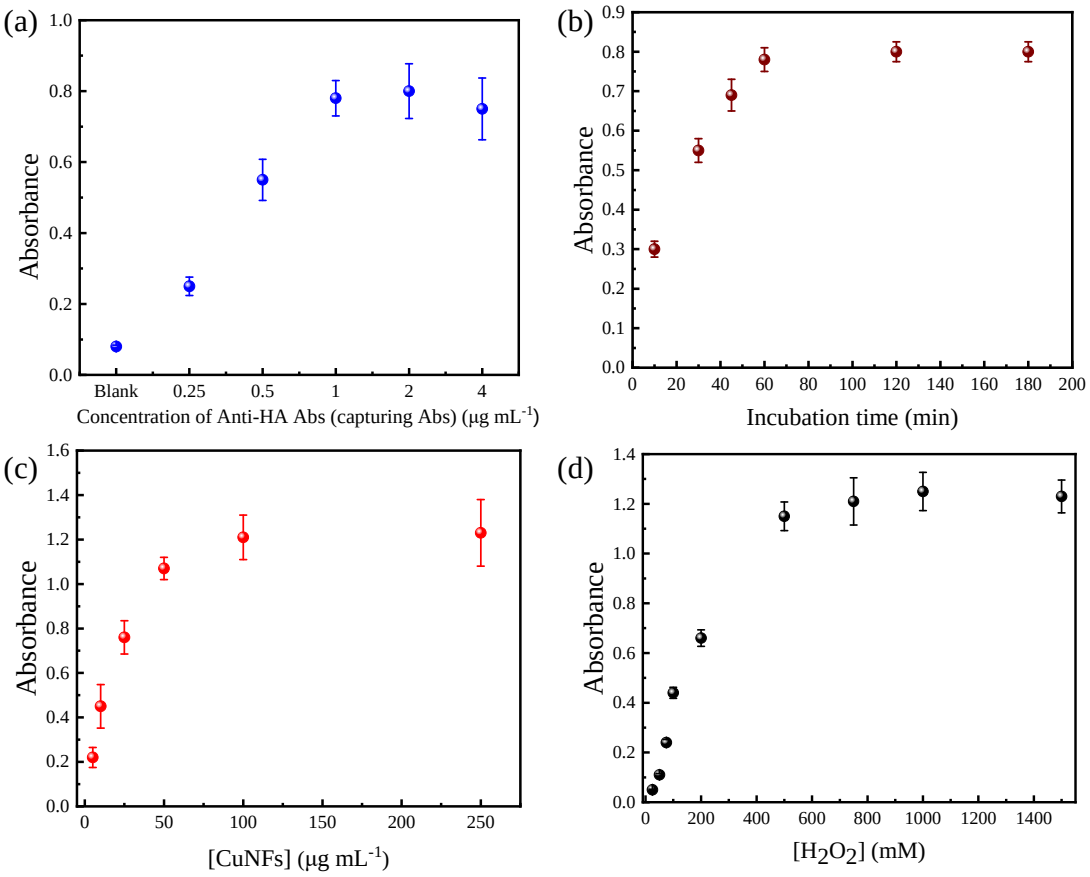

Fig. S1. The optimization of (a) the concentration of capturing antibody, (b) the incubation time of the virus-antibody binding, (c) concentration of the CuNFs and (d) hydrogen peroxide in the developed TMB-NPs@PLGA based method for virus sensing. The concentration of the Influenza virus A/H1N1 was 100 pg mL^{-1}.

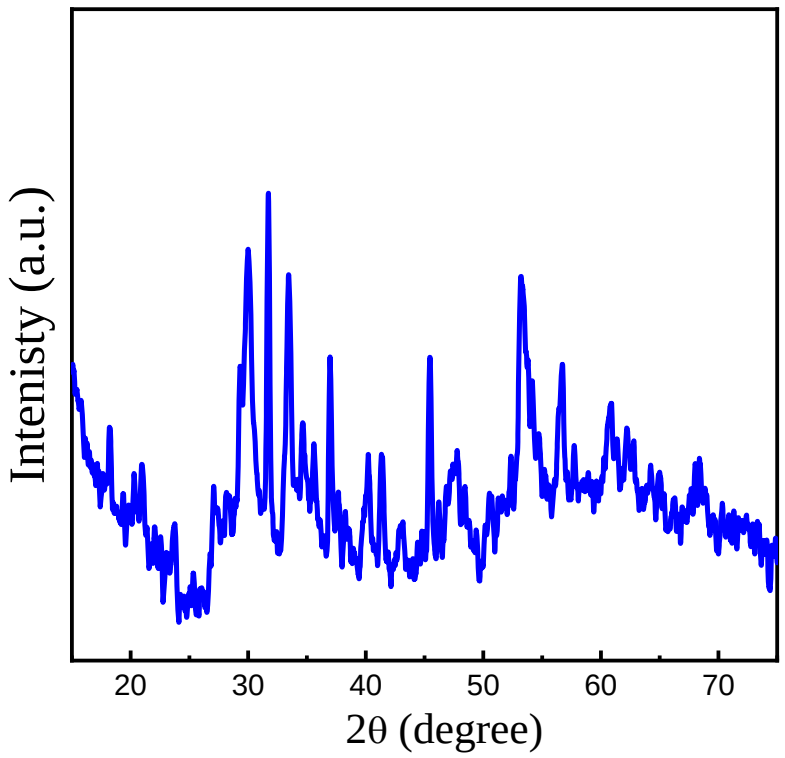

Fig. S2. XRD pattern of CuNFs

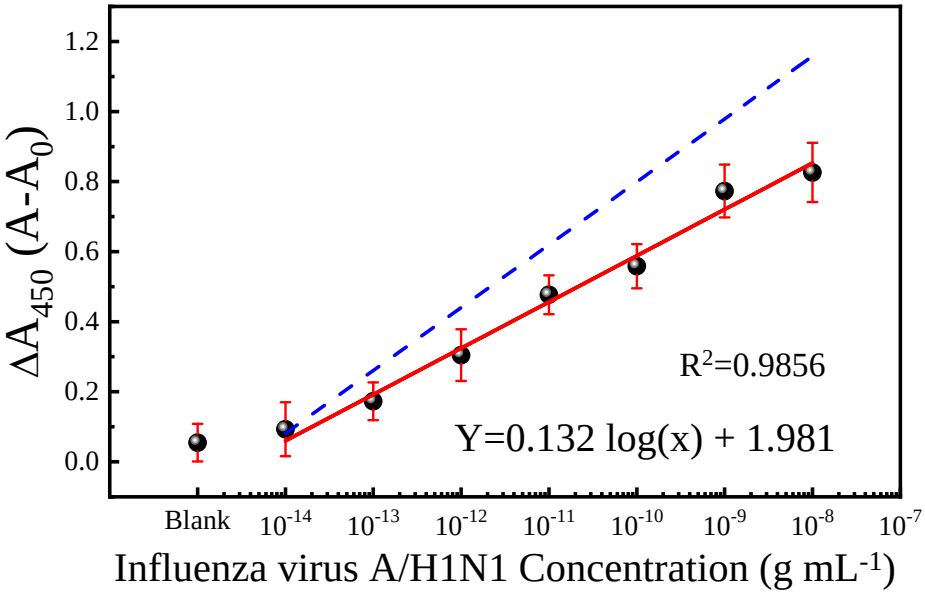

Fig. S3. The calibration line of the IV/A/H1N1 detection by TMB-NPs@PLGA based colorimetric detection. The error bar represents the SD of the triple measurements.

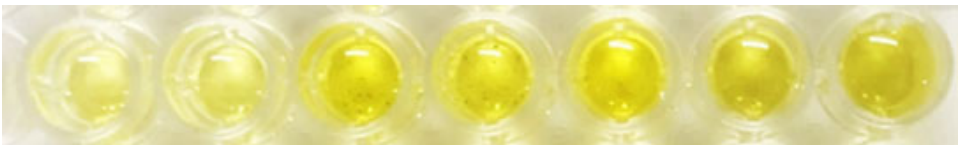

Fig. S4. Digital illustration of the developed color in the Influenza virus A detection using the developed immunoassay

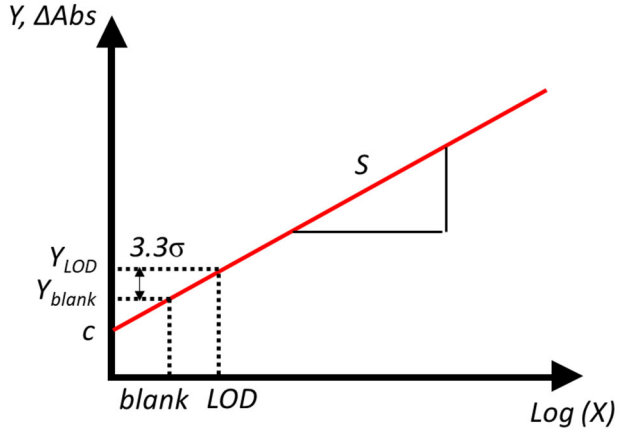

Fig. S5. The illustration of the LOD calculation

References

1. S. R. Ahmed, K. Takemeura, T.-C. Li, N. Kitamoto, T. Tanaka, T. Suzuki and E. Y. Park, Biosens. Bioelectron., 2017, 87, 558–565.
2. T. Wei, D. Du, M.-J. Zhu, Y. Lin and Z. Dai, ACS Appl. Mater. Interfaces, 2016, 8, 6329–6335.
3. Q. Tang, L. Zhang, X. Tan, L. Jiao, Q. Wei and H. Li, Biosens. Bioelectron., 2019, 133, 94–99.
4. S. Oh, J. Kim, V. T. Tran, D. K. Lee, S. R. Ahmed, J. C. Hong, J. Lee, E. Y. Park and J. Lee, ACS Appl. Mater. Interfaces, 2018, 10, 12534–12543.
5. A. B. Ganganboina, A. D. Chowdhury, I. M. Khoris, F. Nasrin, K. Takemura, T. Hara, F. Abe, T. Suzuki and E. Y. Park, Biosensors and Bioelectronics, 2020, 112169.
6. A. B. Ganganboina and R.-A. Doong, Scientific reports, 2019, 9, 1-11.
7. Wu, L., Wan, G., Hu, N., He, Z., Shi, S., Suo, Y., Wang, K., Xu, X., Tang, Y. and Wang, G., Nanomaterials., 2018, 8, 451
8. K. Takemura, O. Adegoke, N. Takahashi, T. Kato, T.-C. Li, N. Kitamoto, T. Tanaka, T. Suzuki and E. Y. Park, Biosens. Bioelectron., 2017, 89, 998–1005.
9. S. R. Ahmed, M. A. Hossain, J. Y. Park, S.-H. Kim, D. Lee, T. Suzuki, J. Lee and E. Y. Park, Biosens. Bioelectron., 2014, 58, 33–39.

10. S. R. Ahmed, J. Kim, T. Suzuki, J. Lee and E. Y. Park, Biotechnol. Bioeng., 2016, 113, 2298–2303.

11. Y.-F. Chang, S.-F. Wang, J. C. Huang, L.-C. Su, L. Yao, Y.-C. Li, S.-C. Wu, Y.-M. A. Chen, J.-P. Hsieh and C. Chou, Biosens. Bioelectron., 2010, 26, 1068–1073.

12. U. Jarocka, R. Sawicka, A. Góra-Sochacka, A. Sirko, W. Zagórski-Ostoja, J. Radecki andH. Radecka, Sensors, 2014, 14, 15714–15728.

13. G.-C. Lee, E.-S. Jeon, W.-S. Kim, D. T. Le, J.-H. Yoo and C.-K. Chong, Virol. J., 2010, 7, 244.